Carbohydrate Polymers 149 (2016) 94–101

Contents lists available at ScienceDirect

Carbohydrate Polymers

journal homepage: www.elsevier.com/locate/carbpol

Maleimide-grafted cellulose nanocrystals as cross-linkers for bionanocomposite hydrogels

C. García-Astrain, K. González, T. Gurrea, O. Guaresti, I. Algar, A. Eceiza, N. Gabilondo*

'Materials + Technologies' Group, Department of Chemical and Environmental Engineering, Polytechnic School, University of the Basque Country, Plaza Europa 1, 20018 Donostia-San Sebastián, Spain

ARTICLE INFO

Article history:
Received 15 December 2015
Received in revised form 15 April 2016
Accepted 20 April 2016
Available online 23 April 2016

Keywords:
Bionanocomposite hydrogel
Diels-Alder
Cellulose nanocrystals
"Click" Chemistry

ABSTRACT

This article deals with the preparation of bionanocomposite hydrogels from natural polymers and nanoentities, an emerging class of materials for biotechnological and biomedical applications. Herein, the applicability of the Diels-Alder "click" reaction to the design of bionanocomposite hydrogels from furan modified gelatin using maleimide-functionalized cellulose nanocrystals as multifunctional cocross-linkers is demonstrated. The functionalization of cellulose nanocrystals with maleimide moieties was confirmed by XPS. The swelling and rheological properties of the resulting bionanocomposite confirmed the formation of hydrogel networks with covalently embedded nanoentities. The Diels-Alder reaction resulted in the formation of stiffer networks with lower swelling ratios due to the formation of additional cross-linking points. The designed "click" strategy proved to be a promising candidate for the formation of fully renewable bionanocomposite hydrogels.

1. Introduction

Hydrogels represent an interesting class of materials with a broad range of applications in the pharmaceutical and biomedical field, as well as in agriculture and cosmetics. Among the different types of hydrogels, hydrogels from bio-derived polymers are particularly interesting since they are easily made biodegradable, promote tissue growth, mimic the extracellular matrix and possess a renewable character (Yang, Han, Duan, Xu, & Sun, 2013; Balakrishnan & Banerjee, 2011; Van Vlierberghe, Dubruel, & Schacht, 2011). During the last decade, the design of bionanocomposite hydrogels including nanoentities such as carbon nanotubes, metallic nanoparticles or clays have attracted great interest from the scientific community (García-Astrain, Ahmed et al., 2015; García-Astrain, Chen et al., 2015; Sabaa, Abdallah, Mohamed, & Mohamed, 2015; Derkus, Emregul, & Emregul, 2015; Haraguchi, 2007). The interactions between the nanoentities and the polymeric matrix at the nanoscale give rise to new materials with enhanced mechanical, thermal, biological, magnetic, optical or electronic properties (García-Astrain, Ahmed et al., 2015; García-Astrain, Chen et al., 2015; Gaharwar, Peppas, & Khademhosseini, 2014; Daniel-da-Silva, Salgueiro, & Trindade, 2013; Kamoun & Menzel, 2012; Shin et al., 2012; Barbucci, Giani, Fedi, Bottari, & Casolaro, 2012; Dvir et al., 2011; Narayana Reddy et al., 2011).

Moreover, in order to achieve superior environmental compatibility as compared to inorganic nanofillers, renewable bionanoentities are being incorporated into novel hydrogel formulations. In particular, cellulose nanocrystals have proven to be effective reinforcements for various hydrogels (Mohammed, Grishkewich, Berry, & Tam, 2015; Araki & Yamanaka, 2014; Dai & Kadla, 2009; McKee et al., 2014; Wallenius et al., 2015). Cellulose nanocrystals (CNCs) are nanoentities 100–500 nm in length and 5–30 nm in width which can be obtained from the partial hydrolysis of a variety of cellulosic materials (Lin & Dufresne, 2014; Yang et al., 2015). This natural nanoscaled material possesses numerous advantages including rod-like morphology, high aspect ratio, crystallinity, non-toxicity, biodegradability, high mechanical strength and surface reactivity (Lin & Dufresne, 2014). Generally, bare CNCs are physically incorporated as reinforcements into the hydrogel matrix (Dai & Kadla, 2009; Mohammed et al., 2015; Wallenius et al., 2015). However, recent work showed that surface-modified CNCs can act both as reinforcement and cross-linking agent within a polymeric matrix. In this way, the performance of the material is improved via the covalent linkage which enhances the interfacial adhesion and reinforces the effect of the filler (Chen, Lin, Huang, & Dufresne, 2015).

* Corresponding author.
E-mail addresses: clara.garcia@ehu.eus (C. García-Astrain), kizkitza.gonzalez@ehu.eus (K. González), taniagurrea@gmail.com (T. Gurrea), olatz.guaresti@ehu.eus (O. Guaresti), itxaso.algar@ehu.eus (I. Algar), arantxa.eceiza@ehu.eus (A. Eceiza), nagore.gabilondo@ehu.eus (N. Gabilondo).

http://dx.doi.org/10.1016/j.carbpol.2016.04.091
0144-8617/

Following this strategy, aldehyde-functionalized CNCs were used as cross-linkers for carboxymethylcellulose/dextran hydrogels and also for the preparation of injectable hyaluronic acid-based formulations (Domingues et al., 2015; Yang, Bakaic, Hoare, & Cranston, 2013). Xylan and gelatin-based hydrogels cross-linked with CNCs or oxidized CNCs, respectively, have also been reported (Köhnke, Elder, Theliander, & Ragauskas, 2014; Dash, Foston, & Ragauskas, 2013). However, to the best of our knowledge, little work has been done on the use of these renewable bionanofillers as hydrogel cross-linkers via means of "click" chemistry.

We have recently reported the applicability of the Diels-Alder (DA) "click" reaction for the preparation of biopolymer-based nanocomposite hydrogels (García-Astrain, Ahmed et al., 2015; García-Astrain, Chen et al., 2015). Herein, we demonstrate the role of maleimide-functionalized CNCs as cross-linkers for the formation of a completely renewable bionanocomposite hydrogel based on gelatin and chondroitin sulfate (CS). Gelatin, composed of a large variety of aminoacids, allows for a broad range of chemical modifications and, due to its sol-gel transition, is a suitable hydrogel precursor (García-Astrain et al., 2014; Van Vlierberghe et al., 2011). On the other hand, CS is a structural component of the extracellular matrix and its use is mainly focused on the synthesis of novel biomaterials.

The aim of this work was to explore the applicability of the Diels-Alder reaction for the preparation of fully biobased nanocomposites using modified CNCs as nanofillers. CNCs were surface-modified by reaction with a maleimide-functionalized aminoacid and the Diels-Alder cycloaddition was then employed as a mild covalent strategy for their binding with furan-modified gelatin. In order to stabilize the hydrogel, second cross-linking based on the amide coupling between CS and gelatin was performed. The effect of functionalized CNCs on the swelling and viscoelastic properties was analyzed, as well as the role of CNCs as stabilizer within this completely renewable bionanocomposite formulation.

2. Materials and methods

2.1. Materials

Gelatin (from porcine skin Type A, 300 Bloom), furfuryl glycidyl ether (FGE, 96.0%), chondroitin sulfate A sodium salt from bovine trachea (CS, 60.0%), *N*-hydroxysuccinimide (NHS, 98.0%), *N*-(3-dimethylaminopropyl)-*N*-ethylcarbodiimide hydrochloride (EDC, 99.0%), β-alanine (99.0%), maleic anhydride (99.0%), 4-(dimethylamino)pyridine (DMAP, 99.0%) and microcrystalline cellulose were purchased from Sigma-Aldrich. Phosphate buffered saline (PBS) solution was prepared from PBS tablets from Panreac (pH = 7.4). Acetic acid, sulphuric acid (96.0%) and ethyl acetate were also purchased from Panreac and toluene and dichloromethane from Lab Scan. Deionized water was employed as solvent. All reagents and solvents were employed as received. Gelatin was modified by reaction of its free ε-amino groups with furfuryl glycidyl ether (FGE) in aqueous solution as described in our previous work (G-FGE) (García-Astrain et al., 2014).

2.2. Synthesis of 3-(2,5-dioxo-2H-pyrrol-1(5H)-yl)propanoic acid (AMI)

AMI was prepared following a reported procedure with some modifications (Scheme 1) (Mantovani et al., 2005). An acetic acid solution of maleic anhydride (5.00 g in 50 mL) was added dropwise to an acetic acid solution of β-alanine (4.54 g in 50 mL). The mixture was stirred for 3 h at room temperature and a white suspension was obtained. After that period, 70 mL of AcOH were added, the temperature was raised until 115 °C and the mixture was stirred overnight. After one hour of reaction a limpid colourless solution was observed. At the end of the whole process, an orange oil was obtained. The solvent excess was removed under reduced pressure and the product was washed with toluene (3 × 30 mL), which was again removed under reduced pressure. The product was then purified by flash chromatography using a silica column (DCM/ethyl acetate 9:1). A white solid was obtained. Yield: 29.15%.

2.3. CNCs functionalization (CNC-Mal)

CNCs were isolated from microcrystalline cellulose after acid hydrolysis with sulfuric acid, removing the disordered or paracrystalline regions of cellulose and leaving crystalline regions intact (González, Retegi, González, Eceiza, & Gabilondo, 2015). 5 g of CNC were hydrolyzed in a water bath at 45 °C using a 64% (w/w) sulfuric acid solution for 30 min. After that time, the solution is poured into a large excess of water and washed with successive centrifugations. The solution was dialyzed against water until neutral pH was reached and finally, nanocrystals were freeze-dried. For the CNC functionalization, 0.5 g of CNC were suspended in 30 mL of *N*,*N*-dimethylformamide (DMF) and 0.5 g of AMI (2.9×10^{-3} mol) were added (Scheme 2) (Cateto & Ragauskas, 2011). The mixture was cooled in ice and 0.399 g of DMAP (3.3×10^{-3} mol) were added at 0 °C. Then, a 10% (w/w) DMF solution containing 0.567 g of EDC (2.9×10^{-3} mol) was added dropwise. The mixture was stirred at room temperature for 24 h. After that time, the surface functionalized CNC (CNC-Mal) were precipitated in a dilute aqueous acid solution and then dialyzed against water until neutral pH was attained. The sample was washed several times with water, ethanol and hydrochloric acid 0.5 M. Finally, the product was recovered after freeze-drying.

2.4. Bionanocomposite preparation

For hydrogel formation, furan modified gelatin (GF, 70 mg) was dissolved in a previously ultrasonicated 0.5 wt.% suspension of maleimide-grafted CNCs. The final concentration of CNC-Mal in the bionanocomposite was 6.3% wt. Finally, CS was incorporated to the mixture (1:2 weight ratio with respect to gelatin) in the presence of EDC (2.3×10^{-3} mol) and NHS (2.0×10^{-3} mol). The mixture was allowed to gel for 24 h (Scheme 3). Control hydrogels without CNCs (G-CS hydrogel) or using bare CNCs (G-CS-CNC hydrogel) were also prepared for comparison following the same procedure described above.

2.5. Methods

Fourier Transform Infrared Spectroscopy (FTIR) was performed in a Nicolet Nexus spectrophotometer at room temperature. KBr pellets were used in the range from 4000 to 400 cm^{-1}, with a 4 cm^{-1} resolution. Proton and carbon Nuclear Magnetic Resonance (^{1}H and ^{13}C NMR) spectra were recorded with an Avance Bruker equipped with BBO z-gradient probe. Experimental conditions were as follows: (a) for ^{13}C NMR: 125.75 MHz, number of scans 14 000, spectral window 25 000 Hz, and recovery delay 2s; (b) for ^{1}H NMR: 500 MHz, number of scans 64, spectral window 5000 Hz, and recovery delay 1s. The solvent employed in all cases was D_2O. X-ray Photoelectron Spectroscopy (XPS) was carried out using a SPECS (Berlin, Germany) system equipped with a Phoibos analyzer 150 1D-DLD and a monochromatic source Al-Kα (1486.7 eV). An initial analysis of the present elements was performed (wide scan: step energy 1 eV, dwell time 0.1 s, pass energy 80 eV) and detailed analysis of the present elements was carried out (detail scan: step energy 0.1 eV, dwell time 0.1 s, pass energy 50 eV) with a take-off angle of 90° for the photoelectron analyser. Curve fitting was performed using a Gaussian–Lorentzian peak shape function with a straight base line throughout the analysis using a CasaXPS software 2.3.16.

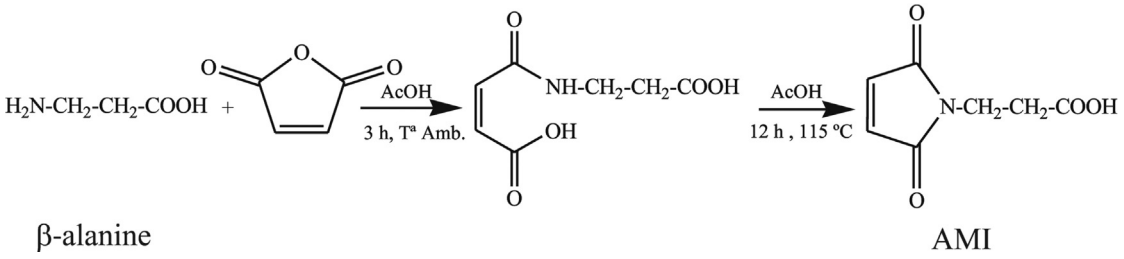

Scheme 1. AMI synthesis from β-alanine and maleic anhydride.

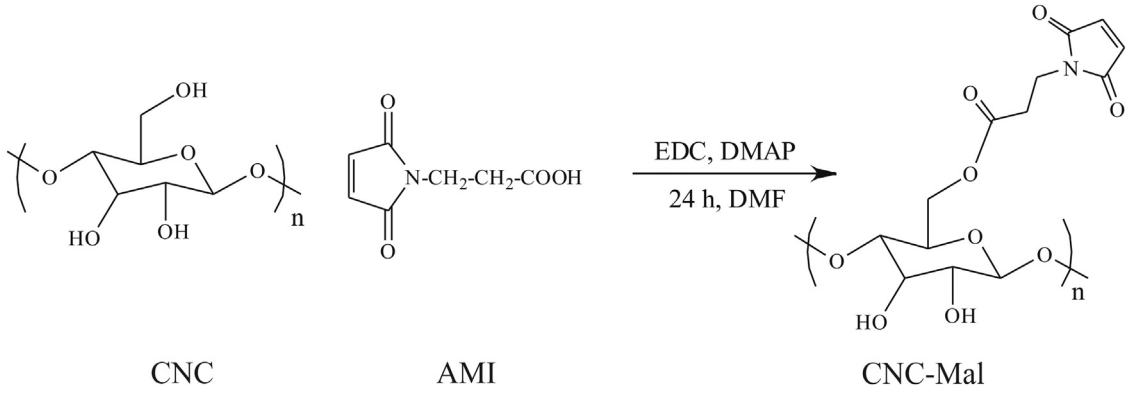

Scheme 2. CNC functionalization using AMI.

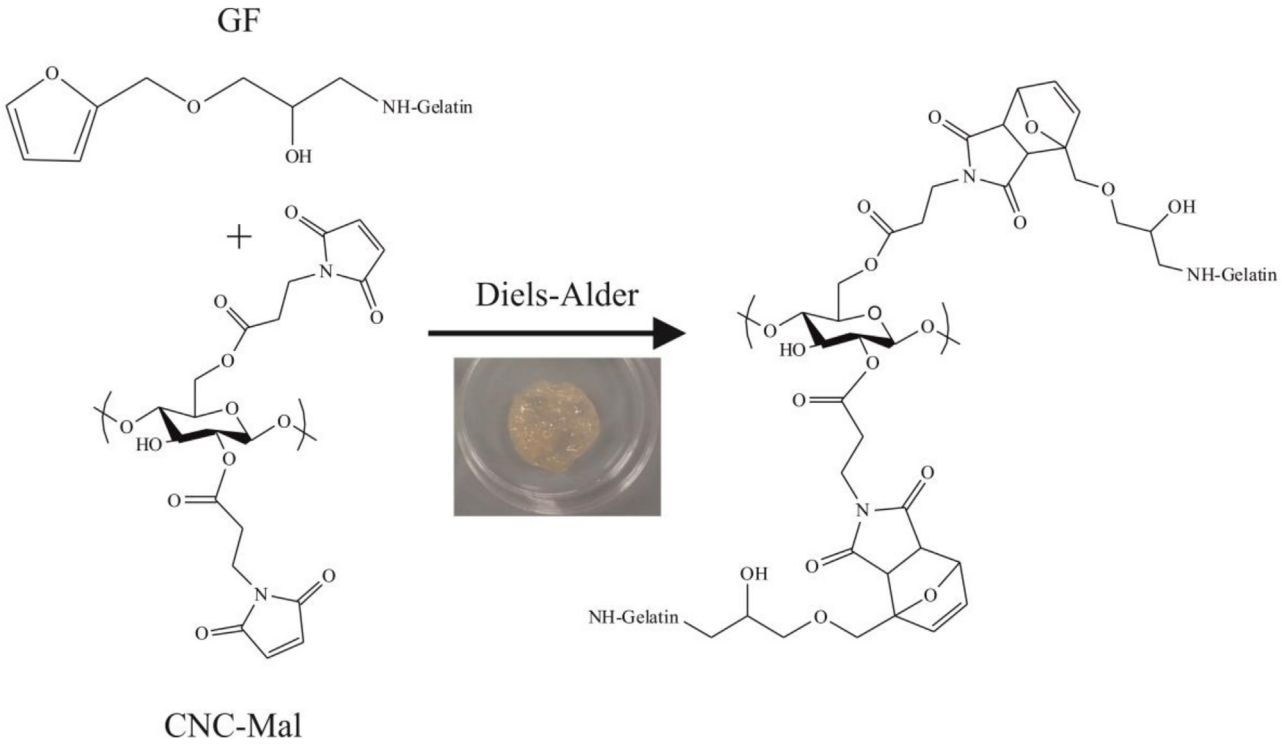

Scheme 3. Diels-Alder reaction between furan-modified gelatin (GF) and CNC-Mal and picture of the hydrogel G-CS-CNC-Mal.

Atomic Force Microscopy (AFM) measurements were performed in tapping mode using a Veeco Multimode scanning probe microscope equipped with a Nanoscope IIIa Controller. All measurements were recorded using TESP type silicon tips having a resonance frequency of approximately 340 kHz and a cantilever spring constant about 40 N m^{-1}. Scanning Electron Microscopy (SEM) experiments were performed by a Hitachi S-2700 SEM at 15 kV accelerating voltage. Freeze-dried samples were sputter-coated with approximately 8 nm of Pt/Au layer to reduce electron charging effects. Dynamic rheological behavior of the hydrogels was analyzed with a Rheometric Scientific Advanced Rheometric Expansion System (ARES), using parallel plate geometry (25 mm diameter). Frequency sweep measurements were performed at 37 °C from 0.1 to 500 rad s^{-1} at a fixed strain in the linear viscoelastic region,

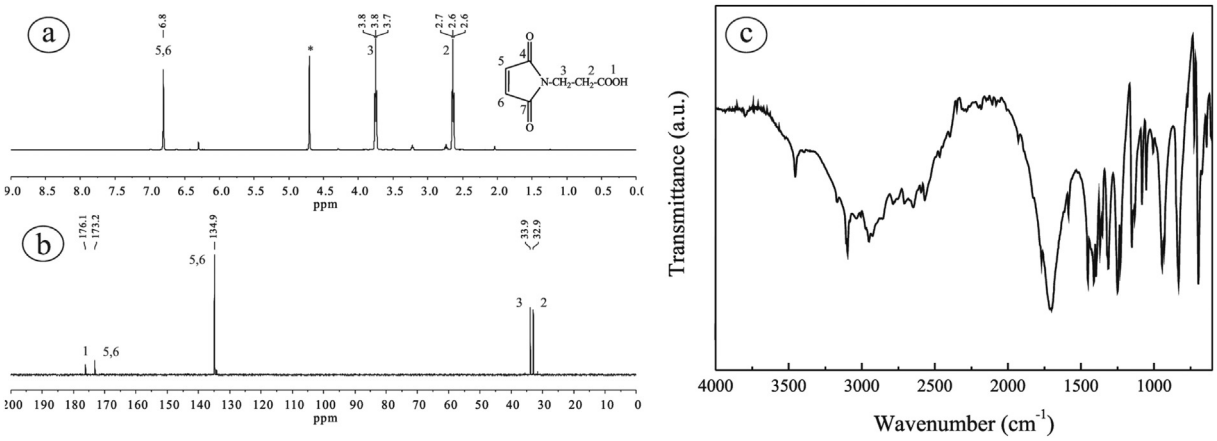

Fig. 1. (a) ^{1}H NMR spectra of AMI in D_2O, (b) ^{13}C NMR spectra of AMI in D_2O and (c) FTIR spectra of AMI.

previously assessed by strain sweep experiments. Hydrogel samples were prepared in the form of disks of 25 mm diameter. Swelling capacity of freeze-dried hydrogels was studied by a general gravimetric method. Samples (n = 3) were incubated at 37 °C in simulated intestinal fluid (phosphate buffer (PBS), pH = 7.4) and water, at selected time intervals the swollen hydrogels were removed, the excess of water absorbed with a filter paper, and weighed. The samples were then dried until constant weight. The swelling ratio (SR) was calculated using Eq. (1):

$$SR(\%) = (W_s - W_d)/W_d \times 100 \quad (1)$$

where W_s is the weight of the swollen sample and W_d is the weight of the dried hydrogel samples. The equilibrium swelling was considered to be achieved when the weight of the hydrogels no longer increased. For degradation studies weighted hydrogel freeze-dried samples were immersed in PBS and incubated at 37 °C for 24 and 48 h. After those times the samples were removed from PBS, dried and weighted. The hydrogel degradation was calculated using Eq. (2):

$$\text{Degradation}(\%) = (m_t/m_0) \times 100 \quad (2)$$

Gel content was determined after swollen hydrogel samples were dried to constant weight, and the percentage conversion was evaluated using Eq. (3):

$$\text{Gel Content}(\%) = (W_t/W_d) \times 100 \quad (3)$$

where W_d is the initial weight of the dry hydrogel sample and W_t is the dry weight of the hydrogel at time t (after incubation in PBS for time t).

3. Results and discussion

3.1. Functionalization of CNC-Mal

CNCs were functionalized with maleimide moieties for the cross-linking of furan-modified gelatin. Maleimide-functionalized CNC-Mal nanocrystals were obtained after the reaction of the hydroxyl groups of CNCs with the carboxylic groups of AMI (Cateto & Ragauskas, 2011; Kalaskar et al., 2008). Maleimide-modified aminoacid derivatives have been employed as bifunctional cross-linkers for the preparation of hydrogels via Diels-Alder reaction (Wei et al., 2010). The incorporation of the maleimide into the AMI structure was confirmed by the peak at 6.81 ppm due to the

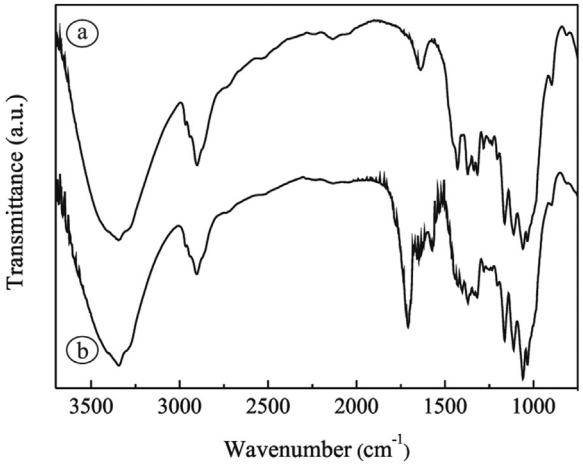

Fig. 2. FTIR spectra of (a) CNCs and (b) CNC-Mal.

—CH=CH— bond of the maleimide ring observed in the ^{1}H NMR spectra (Fig. 1a) (Wei et al., 2010). In the ^{13}C NMR the peaks corresponding to the carbonyl groups and the double bond of the maleimide ring appeared at 173.15 and 134.86 ppm, respectively (Fig. 1b).

Furthermore, at 176.11 ppm the peak corresponding to the carbonyl group of the carboxylic acid can also be observed (Mantovani et al., 2005). The success of the β-alanine modification was also confirmed by FTIR spectroscopy (Fig. 1c). Carbonyl stretching vibration was observed at 1770 and 1709 cm^{-1}. Moreover, the presence of the maleimide ring was revealed by the appearance of bands at 1452 cm^{-1} and at 696 cm^{-1} corresponding to the C=C stretching vibration and alkene bending, respectively (Wei et al., 2010).

The modified aminoacid (AMI) was then used for the surface functionalizaton of the extracted cellulose nanocrystals. The success of the functionalization reaction of CNCs was confirmed by FTIR spectroscopy. Fig. 2 shows the FTIR spectra obtained for CNC and CNC-Mal. It can be observed that the bands corresponding to the stretching vibration of the carbonyl groups present in CNC-Mal appeared at 1709 and 1777 cm^{-1} (Wei et al., 2010). Furthermore, two bands appeared at 1570 and 1400 cm^{-1} corresponding to the C=C and =C—H stretching maleimide vibrations, respectively.

Further confirmation of CNC modification was acquired by XPS analysis. Fig. 3 shows the XPS spectra for non-modified CNC and

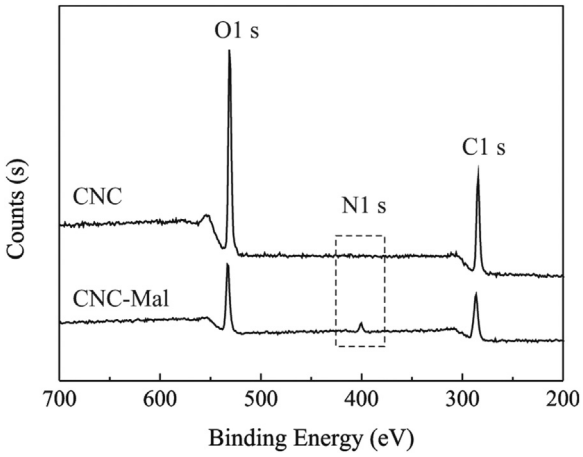

Fig. 3. XPS spectra of CNC and CNC-Mal.

modified CNC-Mal. The XPS spectrum of non-modified CNC presented two peaks in the region of 532 and 286 eV corresponding to oxygen (O) and carbon (C), respectively. After the reaction with AMI, the CNC-Mal samples a third peak near 401 eV attributable to the presence of nitrogen at the surface of the modified nanocrystals (Cateto & Ragauskas, 2011). As expected, after grafting, an increase in the concentration of carbon and nitrogen was observed, which is a clear indication of the grafting of AMI to the CNC surface. XPS data give rise to the determination of the degree of substitution of the surface (DSS) (Missoum, Bras, & Belgacem, 2012). With this technique the degree of substitution of the first nanometers layers can be deduced and the DSS was calculated on basis of nitrogen content (Rueda et al., 2011). From the XPS data, the number of surface-grafted maleimide moieties per glucose unit was estimated and resulted to be 2.2.

Finally, CNCs size and morphology before and after functionalization reaction was studied by AFM. Fig. 4 shows the AFM images of spin-coated aqueous solutions of CNCs and CNC-Mal. As it can be observed, both nanocrystals displayed a fibrilar geometry with a diameter within the nanometric scale (8.5 ± 1.9 nm) and variable length, which indicates that the nanocrystals maintained their integrity. It is worth noting that, as it can be observed in the AFM images, after functionalization, the interactions between the nancocrystals seemed to decrease, since CNC-Mal appeared to be better dispersed with less aggregated entities. This result confirmed the surface maleimide-functionalization which probably hinders hydrogen bonding strong interactions between nanocrystals and, thus, reduces the number of aggregates.

3.2. Hydrogel characterization

As explained before, hydrogels were prepared by reactive mixture of Gel-FGE and chondroitin sulfate, incorporating bare nanocrystals for controls or maleimide-functionalized nanocrystals in case of Diels-Alder nanocomposite hydrogels. Simultaneously, amide coupling between the free amine groups of gelatin, which have not reacted with FGE, and the carboxylic groups of chondroiting sulfate in the presence of EDC and NHS took place. After the reaction, stable hydrogels were obtained. The microstructure of the nanocomposite hydrogels and the control was studied by means of SEM (Fig. 5a–c). For both G-CS-CNC-Mal and G-CS-CNC similar homogeneous compact structures with pits and grooves were observed. In G-CS hydrogel bumps and striated regions in combination with smooth areas were observed. Hydrogels were then characterized in terms of rheological behavior and swelling capacity.

The viscoelastic behavior of the bionanocomposite hydrogel was evaluated by means of frequency sweep rheological experiments. G-CS-CNC-Mal, G-CS-CNC and G-CS hydrogels were submitted to frequency sweep tests at 37 °C at a fixed strain in order to assess

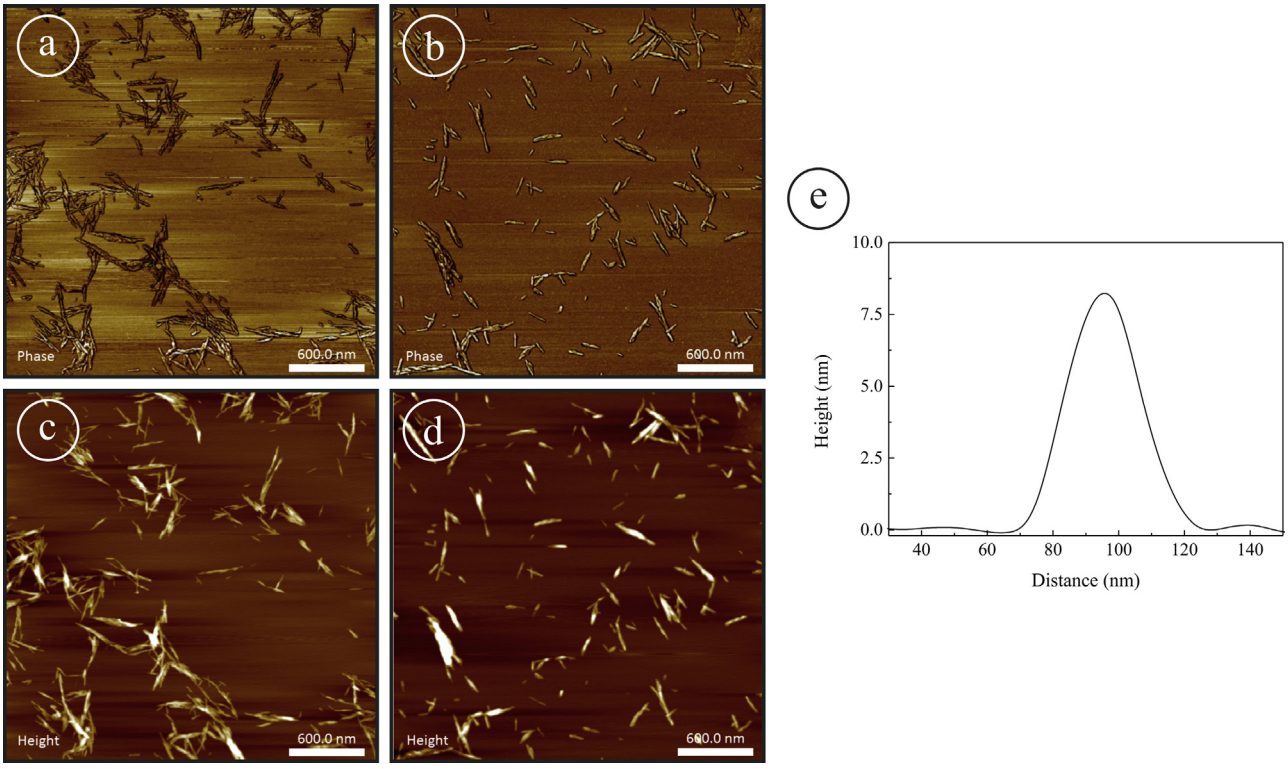

Fig. 4. AFM images of CNC (a) phase image and (c) height image, AFM images of CNC-Mal (b) phase image and (d) height image and (e) height profile of CNC-Mal nanocrystals.

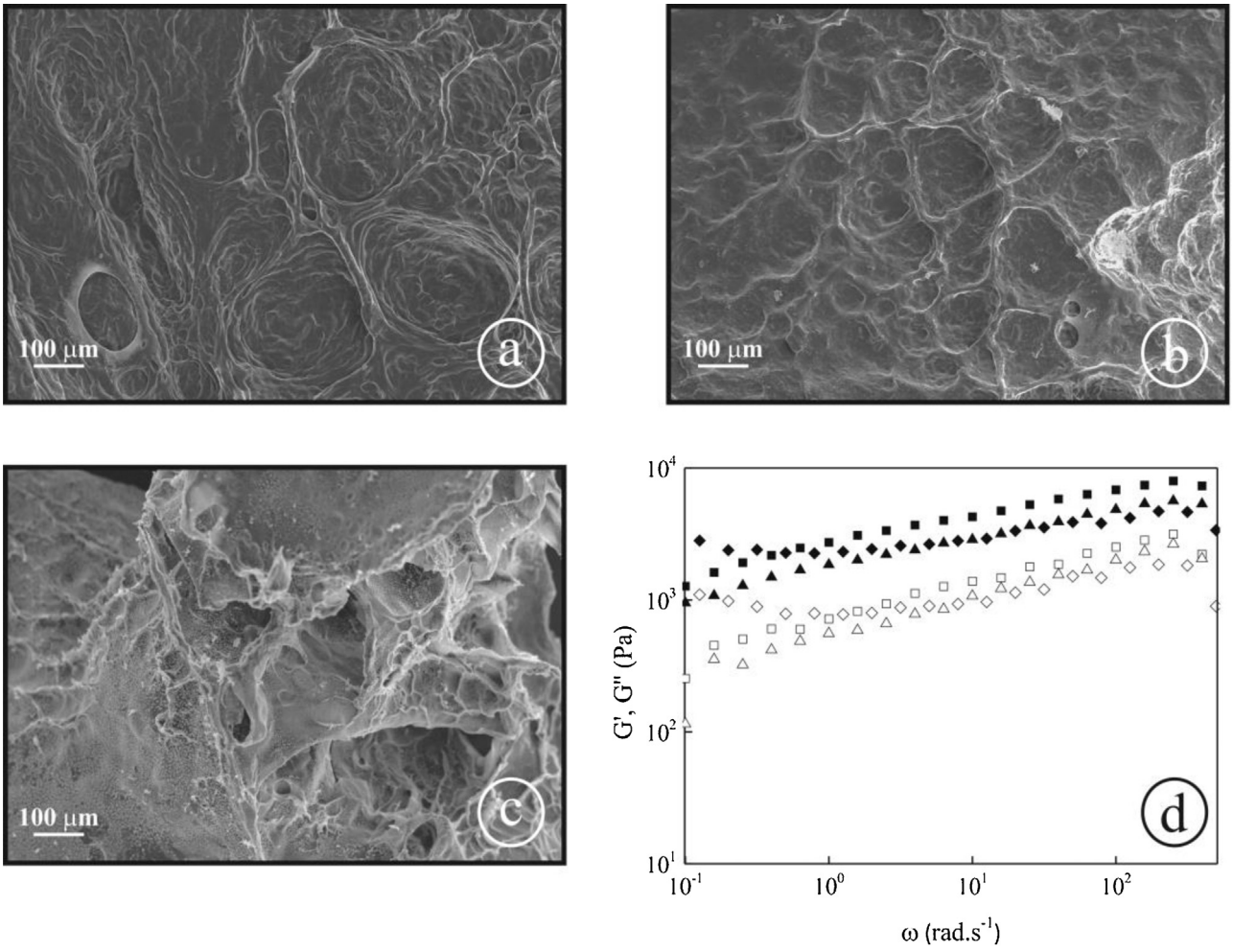

Fig. 5. SEM pictures of a) G-CS-CNC-Mal, b) G-CS-CSN, c) G-CS and b) Frequency sweep of hydrogels (G' (filled symbols) and G" (empty symbols). ■ G-CS-CNC-Mal, ▲G-CS-CNC and ♦ G-CS hydrogels.).

the rheological behavior of the samples. The storage modulus (G') resulted to be higher than the loss modulus (G") and remained almost constant in the frequency range studied, a characteristic of chemically cross-linked networks (Fig. 5). As expected, comparing the different hydrogels, the G' and G" moduli of G-CS were lower than those of CNCs containing hydrogels. In addition, the modulus of G-CS-CNC-Mal bionanocomposite was higher than that of G-CS-CNC, indicating that the covalent attachment of CNC-Mal to furan-modified gelatin resulted in the formation of more cross-linking points and, thus, stiffer networks.

However, as it can be observed in Fig. 5, the mere incorporation of CNCs to the hydrogel formulation resulted in an increase in moduli values as a result of the strong hydrogen bonding interactions between nanocrystals and the two hydrogel forming biopolymers. However, those differences were only appreciated at low frequencies, whereas at higher values both hydrogels (G-CS and G-CS-CNC) presented almost identical storage moduli values. On the contrary, G-CS-CNC-Mal hydrogel presented higher G' values in the entire range of frequency, indicating the formation of stiffer hydrogels that maintained their improved properties due to the participation of the covalently clicked nanocrystals. The cross-linking density (ρ_c) of the different hydrogels was calculated from the rheological data, since the storage modulus is related to the cross-linking density according to the already reported Eq. (3) (Hajighasem & Kabiri, 2013; Jiang, Su, Mather, & Bunning, 1999; Shet Hui Wong, Ashton, & Dodou, 2015):

$$G' = \rho_c RT \quad (3)$$

where R is the gas constant and T the temperature. The resulting values were 1.55, 1.04 and 1.09 mol $m^{-3}$for G-CS-CNC-Mal, G-CS-CNC and G-CS, respectively. As it can be observed, the used of functionalized CNCs in G-CS-CNC-Mal resulted in the formation of more cross-linked networks due to the covalent attachment of CNC-Mal to furan-modified gelatin.

Finally, the swelling capacity (SR) of the hydrogels was assessed as a function of the incubation time in PBS and water at 37 °C (Fig. 6a). It is well known that the swelling ratio of hydrogels depends on the cross-linking density of the polymeric network, the hydrophilic character of the polymers and their concentration (García-Astrain et al., 2014). During hydrogel swelling, the polymeric chains imbibe the solution which starts to permeate inside the hydrogel, this process being restricted by the network cross-linking. As it can be seen, the lowest SR value was recorded for the G-CS-CNC-Mal hydrogel both in water and PBS (2200 ± 210% and 862 ± 28%, respectively). Similar SR values were recorded for G-CS and G-CS-CNC hydrogels in PBS (1100 ± 18% and 1156 ± 19%, respectively). In water, G-CS-CNC SR was higher than that of G-CS, probably due to the hydrophilic nature of the CNCs (3220 ± 224% and 2463 ± 31%, respectively). These results confirmed again the

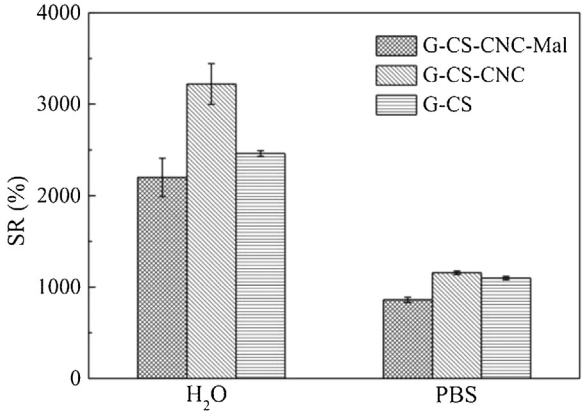

Fig. 6. Equilibrium SR of hydrogels in H_2O and PBS at 37 °C.

Table 1
Degradation of the different hydrogel samples in PBS at 37 °C.

Sample	Degradation (%)	
	24 h	48 h
G-CS-CNC-Mal	13	77
G-CS-CNC	28	70
G-CS	28	41

important role of CNC-Mal as cross-linker for gelatin chains, since more cross-linked networks usually display lower swelling ratios (García-Astrain, Ahmed et al., 2015).

The gel contents of the different hydrogels were found in the range of 87–72%; this indicated the applicability of an effective cross-linking method for hydrogel preparation. The swelling ratio in PBS solution at 37 °C was also recorded for longer time periods (24 and 48 h) in order to evaluate the stability against hydrolytic degradation of the bionanocomposites. The degradation results, calculated using Eq. (2), are shown in Table 1. The results suggested that the incorporation of reactive functionalized CNCs resulted in more stable hydrogels after shorter incubation periods, when comparing with hydrogels containing only bare CNCs. However, after longer incubation periods, the incorporation of both bare CNCs and maleimide-modified CNCs favoured the degradation. The high hydrophilic nature of CNCs could be responsible for this behavior and the hydrolytic decomposition of the network could be favoured by the hydrophilicity of the hydrogel components (Moeinzadeh & Jabbari, 2015). These results suggest the typical hydrolytic cleavage of ether and ester linkages within the hydrogel network (Jiang et al., 2015; Lee, Park, & Ki, 2016; Pradal, Grøndahl, & Cooper-White, 2015). This ether and ester bonds are present between gelatin and furan groups and between CNC and maleimide groups and allowed the hydrolytic break of the overall network structure in PBS with time. Nevertheless, for short incubation periods the incorporation of CNC-Mal and the formation of additional cross-linking points due to the Diels-Alder reaction resulted in more stable hydrogels over time. Under the studied conditions, the degradation could only be attributed to hydrolytic processes, which resulted in partial solubilization of the samples. Under real physiological conditions, where enzymes or other reagents are present, the rate and extent of degradation would probably increase (Yu, Cao, Zeng, Zhang, & Chen, 2013).

4. Conclusions

A bionanocomposite hydrogel based on gelatin and chondroitin sulfate and containing covalently bound maleimide-functionalized CNCs was prepared. Functionalized CNCs were used as cross-linkers via Diels-Alder "click" cycloaddition to furan-modified gelatin. The role of CNCs as cross-linkers for gelatin was confirmed by swelling and rheological measurements. Typically, higher storage moduli values were recorded for the cross-linked bionanocomposite when comparing with the controls. Moreover, changes in the swelling properties of the hybrid hydrogels were attributed to the formation of additional cross-linking points due to the presence of functionalized CNCs. This synthetic strategy proved to be a suitable alternative for the preparation of biobased hydrogels with tailored properties and obtained completely from renewable resources which may lead to materials with potential applications in the biomedical field.

Acknowledgements

Financial support from the GV/EJ Grupos Consolidados (IT-776-13) and Domingo Martínez Foundation is acknowledged. C. García-Astrain wishes to acknowledge the Universidad del País Vasco/Euskal Herriko Unibertsitatea (Ayudas para la Formación de Personal Investigador) for PhD grant PIFUPV10/034. Technical and human support provided by SGIker (UPV/EHU, MICINN, GV/EJ, ERDF and ESF) is also gratefully acknowledged.

References

Araki, J., & Yamanaka, Y. (2014). Anionic and cationic nanocomposite hydrogels reinforced with cellulose and chitin nanowhiskers: effect of electrolyte concentration on mechanical properties and swelling behaviours. *Polymers for Advanced Technologies*, *25*, 1108–1115.
Balakrishnan, B., & Banerjee, R. (2011). Biopolymer-based hydrogels for cartilage tissue-engineering. *Chemical Reviews*, *111*, 4453–4474.
Barbucci, R., Giani, G., Fedi, S., Bottari, S., & Casolaro, M. (2012). Biohydrogels with magnetic nanoparticles as cross-linker: characteristics and potential use for controlled antitumor drug-delivery. *Acta Biomaterialia*, *8*, 4244–4252.
Cateto, C. A., & Ragauskas, A. (2011). Amino acid modified cellulose whiskers. *RSC Advances*, *1*, 1695–1697.
Chen, J., Lin, N., Huang, J., & Dufresne, A. (2015). Highly alkynyl-functionalization of cellulose nanocrystals and advanced nanocomposites thereof via click chemistry. *Polymer Chemistry*, *6*, 4385–4395.
Dai, Q., & Kadla, J. F. (2009). Effect of nanofillers on carboxymethyl cellulose/hydroxyethyl cellulose hydrogels. *Journal of Applied Polymer Science*, *114*, 1664–1669.
Daniel-da-Silva, A. L., Salgueiro, A. M., & Trindade, T. (2013). Effects of Au nanoparticles on thermoresponsive genipin-crosslinked gelatine hydrogels. *Gold Bulletin*, *46*, 25–33.
Dash, R., Foston, M., & Ragauskas, A. J. (2013). Improving the mechanical and thermal properties of gelatin hydrogels cross-linked by cellulose nanowhiskers. *Carbohydrate Polymers*, *91*, 638–645.
Derkus, B., Emregul, K. C., & Emregul, E. (2015). Evaluation of protein immobilization capacity on various carbon nanotube embedded hydrogel biomaterials. *Materials Science and Engineering: C*, *56*, 132–140.
Domingues, R. M. A., Silva, M., Gershovich, P., Betta, S., Babo, P., Caridade, S. G., et al. (2015). Development of injectable hyaluronic acid/cellulose nanocrystals bionanocomposite hydrogels for tissue engineering applications. *Bioconjugate Chemistry*, *26*, 1571–1581.
Dvir, T., Timko, B. P., Brigham, M. D., Naik, S. R., Karajanagi, S. S., Levy, O., et al. (2011). Nanowired three-dimensional cardiac patches. *Nature Nanotechnology*, *6*, 720–725.
Gaharwar, A. K., Peppas, N. A., & Khademhosseini, A. (2014). Nanocomposite hydrogels for biomedical applications. *Biotechnology and Bioengineering*, *111*, 441–453.
García-Astrain, C., Ahmed, I., Kendziora, D., Guaresti, O., Eceiza, A., Fruk, L., et al. (2015). Effect of maleimide-functionalized gold nanoparticles on hybrid biohydrogels properties. *RSC Advances*, *5*, 50268–50277.
García-Astrain, C., Chen, C., Burón, M., Palomares, T., Eceiza, A., Fruk, L., et al. (2015). Biocompatible hydrogel nanocomposite with covalently embedded silver nanoparticles. *Biomacromolecules*, *16*, 1301–1310.
García-Astrain, C., Gandini, A., Peña, C., Algar, I., Eceiza, A., Corcuera, M., et al. (2014). Diels–Alder click chemistry for the cross-linking of furfuryl-gelatin-polyetheramine hydrogels. *RSC Advances*, *4*, 35578–35587.
González, K., Retegi, A., González, A., Eceiza, A., & Gabilondo, N. (2015). Starch and cellulose nanocrystals together into thermoplastic starch bionanocomposites. *Carbohydrate Polymers*, *117*, 83–90.
Hajighasem, A., & Kabiri, K. (2013). Cationic highly alcohol-swellable gels: synthesis and characterization. *Journal of Polymer Research*, *20*, 218–227.
Haraguchi, K. (2007). Nanocomposite hydrogels. *Current Opinion in Solid State and Materials Science*, *11*, 47–54.
Jiang, H., Qin, S., Dong, H., Lei, Q., Su, X., Zhuo, R., et al. (2015). An injectable and fast-degradable poly(ethylene glycol) hydrogel fabricated via bioorthogonal

strain-promoted azide-alkyne cycloaddition click chemistry. *Soft Matter*, *11*, 6029–6036.
Jiang, H., Su, W., Mather, P. T., & Bunning, T. J. (1999). Rheology of highly swollen chitosan/polyacrylate hydrogels. *Polymer*, *40*, 4593–4602.
Köhnke, T., Elder, T., Theliander, H., & Ragauskas, A. J. (2014). Ice template and cross-linked xylan/nanocrystalline cellulose hydrogels. *Carbohydrate Polymers*, *100*, 24–30.
Kalaskar, D. M., Gough, J. E., Uljin, R. V., Sampson, W. W., Scurr, D. J., Rutten, F. J., et al. (2008). Controlling cell morphology on amino acid-modified cellulose. *Soft Matter*, *4*, 1059–1065.
Kamoun, E. A., & Menzel, H. (2012). HES-HEMA nanocomposite polymer hydrogels: swelling behavior and characterization. *Journal of Polymer Research*, *19*, 9851–9865.
Lee, S., Park, Y. H., & Ki, C. S. (2016). Fabrication of PEG–carboxymethylcellulose hydrogelby thiol-norbornene photo-click chemistry. *International Journal of Biological Macromolecules*, *83*, 1–8.
Lin, N., & Dufresne, A. (2014). Nanocellulose in biomedicine: current status and future prospect. *European Polymer Journal*, *59*, 302–325.
Mantovani, G., Lecolley, F., Tao, L., Haddleton, D. M., Clerx, J., Cornelissen, J. J. L. M., et al. (2005). Design and synthesis of *N*-maleimido-functionalized hydrophilic polimers via copper-mediated living radical polimerization: a suitable alternative to PEGylation chemistry. *Journal of the American Chemical Society*, *127*, 2966–2973.
McKee, J. R., Hietala, S., Seitsonen, J., Laine, J., Kontturi, E., & Ikkala, O. (2014). Thermoresponsive nanocellulose hydrogels with tunable mechanical properties. *ACS Macro Letters*, *3*, 266–270.
Missoum, K., Bras, J., & Belgacem, M. N. (2012). Organization of aliphatic chains grafted on nanofibrillated cellulose and influence on final properties. *Cellulose*, *19*, 1957–1973.
Moeinzadeh, S., & Jabbari, E. (2015). Gelation characteristics, physic-mechanical properties and degradation kinetics of micellar hydrogels. *European Polymer Journal*, *72*, 566–576.
Mohammed, N., Grishkewich, N., Berry, R. M., & Tam, K. C. (2015). Cellulose nanocrystal–alginate hydrogel beads as novel adsorbents for organic dyes in aqueous solutions. *Cellulose*, *22*, 3725–3738.
Narayana Reddy, N., Varaprasad, K., Ravindra, S., Subba Reddy, G. V., Reddy, K. M. S., Mohan Reddy, K. M., et al. (2011). Evaluation of blood compatibility and drug release studies of gelatin based magnetic hydrogel nanocomposites. *Colloid and Surfaces A: Physicochemical and Engineering Aspects*, *385*, 20–27.
Pradal, C., Grondahl, L., & Cooper-White, J. (2015). Hydrolytically degradable polyrotaxane hydrogels for drug and cell delivery applications. *Biomacromolecules*, *16*, 389–403.
Rueda, L., Fernandez d'Arlas, B., Zhou, Q., Berglund, L. A., Corucera, M. A., Mondragon, I., et al. (2011). Isocyanate-rich cellulose nanocrystals and their selective insertion in elastomeric polyurethane. *Composites Science and Technology*, *71*, 1953–1960.
Sabaa, M. W., Abdallah, H. M., Mohamed, N. A., & Mohamed, R. R. (2015). Synthesis, characterization and application of biodegradable crosslinked carboxymethyl chitosan/poly(vinyl alcohol) clay nanocomposites. *Materials Science and Engineering: C*, *56*, 363–373.
Shet Hui Wong, R., Ashton, M., & Dodou, K. (2015). Effect of crosslinking agent concentration on the properties of unmedicated hydrogels. *Pharmaceutics*, *7*, 305–319.
Shin, S. R., Bae, H., Cha, J. M., Mun, J. Y., Chen, Y. C., Tekin, H., et al. (2012). Carbon nanotube reinforced hybrid microgels as scaffold materials for cell encapsulation. *ACS Nano*, *6*, 362–372.
Van Vlierberghe, S., Dubruel, P., & Schacht, E. (2011). Biopolymer-based hydrogels as scaffolds for tissue engineering applications: a review. *Biomacromolecules*, *12*, 1387–1408.
Wallenius, J., Pahimanolis, N., Zoppe, J., Kilpeläinen, P., Master, E., Ilvesniemi, H., et al. (2015). Continuous propionic acid production with Propionibacterium acidipropionici immobilized in a novel xylan hydrogel matrix. *Bioresource Technology*, *197*, 1–6.
Wei, H. L., Yang, Z., Chu, H. J., Zhu, J., Li, Z. C., & Cui, J. S. (2010). Facile preparation of poly(*N*-isopropylacrylamide)-based hydrogels via aqueous Diels-Alder click reaction. *Polymer*, *51*, 1694–1702.
Yang, D., Peng, X., Zhong, L., Cao, X., Chen, W., Wang, S., et al. (2015). Fabrication of a highly elastic nanocomposite hydrogel by surface modification of cellulose nanocrystals. *RSC Advances*, *5*, 13878–13885.
Yang, J., Han, C. R., Duan, J. F., Xu, F., & Sun, R. C. (2013). Mechanical and viscoelastic properties of cellulose nanocrystals reinforced poly(ethylene glycol) nanocomposite hydrogels. *ACS Applied Materials and Interfaces*, *5*, 3199–3207.
Yang, X., Bakaic, E., Hoare, T., & Cranston, E. D. (2013). Injectable polysaccharide hydrogels reinforced with cellulose nanocrystals: morphology, rheology, degradation, and cytotoxicity. *Biomacromolecules*, *14*, 4447–4455.
Yu, F., Cao, X., Zeng, L., Zhang, Q., & Chen, X. (2013). An interpenetrating HA/G/CS biomimic hydrogel via Diels-Alder click chemistry for cartilage tissue engineering. *Carbohydrate Polymers*, *97*, 188–195.